Research Article | Vol. 29, No. 8 / 12 April 2021 / Optics Express 11372

Optics EXPRESS

Demonstration of optical gain at 1550 nm in an Er^{3+}-Yb^{3+} co-doped phosphate planar waveguide under commercial and convenient LED pumping

WANG FAN, BAOPING ZHANG, CE WANG, LEIYING YING, XINGCHEN YANG, ZHAOQIN ZHOU, AND DAN ZHANG*

School of Electronic Science and Engineering (National Model Microelectronics College), Xiamen University, Xiamen 361005, China

*zhangdan@xmu.edu.cn

Abstract: A 980 nm semiconductor laser is always selected as the pump source for erbium-ytterbium co-doped optical waveguide amplifiers. In this work, two low-cost blue-violet LEDs, rather than an expensive 980 nm laser, were used to pump an Er^{3+}-Yb^{3+} co-doped phosphate planar waveguide. When the signal power was 0.4 mW at a 1550 nm wavelength, internal optical gains of about 4.1 and 4.5 dB/cm were respectively obtained under the excitations of a 32 mW/cm^2, 275 nm LED and a 914 mW/cm^2, 405 nm LED. It was found that 51.17% of the total Er^{3+} ions in the $^2H_{9/2}$ state contributed to the luminescence at 1550 nm, and a theoretical model of gain simulation was established under the excitation of a 405 nm LED. The calculated gain of about 4.1 dB/cm was found to be in accordance with the experimental optical gain results.

1. Introduction

Rare earth-doped optical waveguide amplifiers (RDWAs) have played an important role in the development of optoelectronics and integrated optics [1–3]. They can be integrated with other photonic devices, such as optical switches, optical modulators and arrayed waveguide gratings to compensate for optical loss. Compared with other RDWAs, erbium-ytterbium co-doped optical waveguide amplifiers (EYDWAs) have received substantial attention because they can be applied to the third standard communication window at the wavelength of 1550 nm [4,5]. Usually, inorganic host materials, such as crystals, silicate, phosphate, alumina, lithium niobate, and polymers or organic-inorganic hybrid materials (OIHMs), can also be used to fabricate EYDWAs. Compared to organic EYDWAs, inorganic EYDWAs are favored by researchers due to their advantages including a higher doping concentration, lower waveguide loss, and excellent thermal stability. The pertinent fabrication technologies, such as the ion exchange method and ion implantation process, have been well developed. However, in the development process of EYDWAs, researchers have mainly focused on the structure design of the devices [6,7] and the innovation of new materials [8,9]. Regarding the pumping source of EYDWAs, a 980 nm laser diode (LD) is always selected and coupled with a 1550 nm signal laser to input from one end of the waveguide. Almost all the results of the optical gain experiments and the atomic rate equations established in theory are based on laser pumping method [10,11]. However, there are some disadvantages to 980 nm laser pumping. First, a wavelength division multiplexer (WDM) required to couple the 980 nm laser with the 1550 nm signal laser, which introduces additional optical loss. Moreover, the intrinsic absorption cross-sections of Er^{3+} ions at 980 nm are on the order of 10^{-24} and 10^{-25} m^2, which often requires higher pump power (100-400 mW) [12,13], thereby causing the energy upconversion effect of Er^{3+} ions [14] and thermal damage of waveguides. Furthermore, the optical power density at the input end of the waveguide can reach to about 10^5 W/cm^2 (100 mW pump power on the 9×9 µm cross-section of the waveguide),

#414847 https://doi.org/10.1364/OE.414847
Journal © 2021 Received 25 Nov 2020; revised 13 Mar 2021; accepted 17 Mar 2021; published 29 Mar 2021

Optics EXPRESS

which could destroy the waveguide and affect the thermal stability of the device [15,16]. Also, an expensive 980 nm laser will increase the commercial cost of the device.

There are some advantages to replacing the 980 nm LD with an LED as the pump source. Because an LED can be placed vertically in the top space of the waveguide, the EYDWA can be flexibly placed in any position of the planar optical interconnection, thereby allowing it to be integrated with other optical devices in configurations other than a one-dimensional axis, which is required under the excitation of the 980 nm LD. Figure 1(a) illustrates the method of a 980 nm LD coupled into the waveguide via the end face of the WDM, which is the traditional measurement method for EYDWAs. Figure 1(b) illustrates the vertical top-pumping mode of a blue-violet LED, which is the optical gain measurement method proposed in this work, the stability of the system is higher and its operation is convenient. In addition, the intensity of the LED distributes uniformly along the waveguide, and will not decrease with the increase of the waveguide length; thus, it will achieve a higher gain under a lower pump power. In 2005, Lee *et al.* demonstrated an optical gain of 3 dB/cm at a 1.5 μm wavelength in a Si-nanocrystal-sensitized, Er-doped silica waveguide using a 470 nm LED [17]. In the same year, Lee *et al.* constructed a theoretical model and calculated a gain of 10 dB/cm when pumping with a 470 nm LED [18]. In 2009, Dahal reported EDWAs operating near 1.54 μm based on the III-N material system and obtained a relative optical gain of 8 dB by pumping with a 365 nm LED [19]. In 2015, Li *et al.* proposed the possibility of using an LED as the pump source, but experimental data were not provided [20].

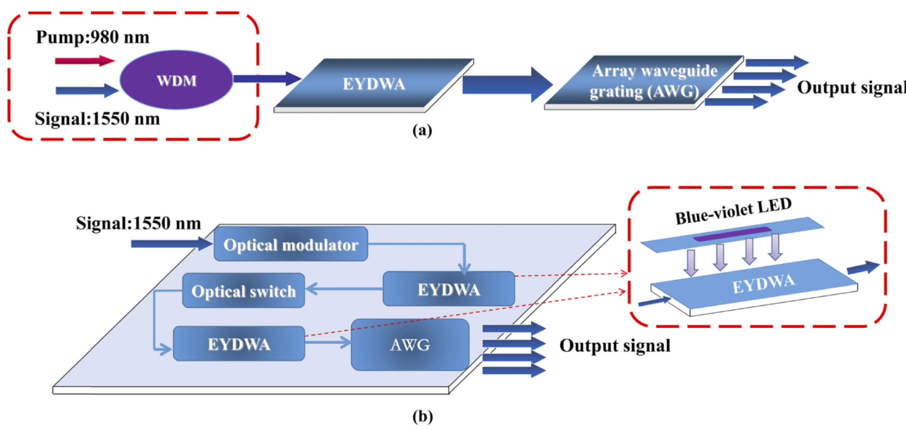

Fig. 1. The schematic diagram of EYDWAs in the field of on-chip optical integration. (a) Under traditional 980 nm LD pumping, optical fiber waveguide axial coupling is adopted, which requires WDM combination signals. (b) In the proposed method, the EYDWAs are pumped with a blue-violet LED, which is conducive to planar photon integration.

In this work, two inexpensive LEDs, instead of an expensive 980 nm laser, were used to pump an Er^{3+}-Yb^{3+} co-doped phosphate planar waveguide. The experimental results demonstrate that when the signal power was 0.4 mW at a wavelength of 1550 nm, internal optical gains of 4.1 and 4.5 dB/cm were respectively obtained under the excitation of a 32 mW/cm^2, 275 nm LED and a 914 mW/cm^2, 405 nm LED. Additionally, an optical gain of 5.2 dB was achieved when the signal power was 0.2 mW. The luminescence mechanism of Er^{3+} ions based on the pumping of a 405 nm LED was demonstrated. Moreover, a theoretical model of gain calculation under 405 nm LED pumping was established, and a gain of 4.1 dB/cm was obtained by theoretical simulation, which was consistent with the gain obtained by the experiment. Finally, the relationships between the gain performance and the waveguide size, pump power density, and absorption cross-section are discussed.

The findings of this research can help to overcome the thermal damage of the waveguide caused by high power, and can decrease the optical losses introduced by the WDM under the excitation of a 980 nm LD. Without this commercial LED pumping source, it is difficult to reduce the commercial cost and technological difficulties of optical integration. The vertical top-pumping mode of blue-violet LEDs for EYDWAs will drive future development in the field of on-chip optical integration.

2. Experimental details

Erbium-ytterbium co-doped phosphate glass with dimensions of 10×12×2 mm, which was purchased from Metalaser Company in China, was used in the experiment. It contains 2 wt% Er_2O_3, 4 wt% Yb_2O_3 and other inorganic oxides such as P_2O_5, Al_2O_3, and Na_2O-K_2O-BaO, and the concentrations of Er^{3+} and Yb^{3+} ions are respectively 1.616×10^{20} and 3.14×10^{20} cm^{-3}. The radiative lifetime of Er^{3+} ions at the $^4I_{13/2}$ level is about 9.97 ms. When a single-mode fiber with a core diameter of 9 µm is incident from one end of the glass, for a transmission length of 10 mm, it can be approximately considered that the optical signal is transmitted in a planar waveguide with a limited cross-section of 9×9 µm. The air was regarded as the cladding. The refractive indexes of the Er^{3+}-Yb^{3+} co-doped phosphate glass at wavelengths of 1550 nm and 405 nm are respectively 1.528 and 1.537. A 275 nm LED and a 405 nm LED were respectively used to replace the expensive 980 nm LD as the pump source. The absorption spectrum was recorded with a Shimdazu UV3600 UV-Vis-NIR spectrophotometer and the optical gain of the planar waveguide was measured by an Ocean Optics FLAME-NIR-INTSMA25 optical spectrometer. All measurements were carried out at room temperature.

3. Results

3.1. Absorption properties

Figure 2 presents the absorption spectrum of the Er^{3+}-Yb^{3+} co-doped phosphate glass. The absorption bands at wavelengths of 365, 375, 405, 450, 488, 520, 544, 650, 808, 975, and 1535 nm, which respectively correspond to $^4I_{15/2}\rightarrow{}^4G_{9/2}$, $^4G_{11/2}$, $^2H_{9/2}$, $^4F_{5/2}$, $^4F_{7/2}$, $^2H_{11/2}$, $^4S_{3/2}$, $^4F_{9/2}$, $^4I_{9/2}$, $^4I_{11/2}$, and $^4I_{13/2}$, are the intrinsic absorption peaks of Er^{3+} ions [21]. Among them, the absorption band at the wavelength of 975 nm also corresponds to the $^2F_{7/2}\rightarrow{}^2F_{5/2}$ transition of Yb^{3+} ions. The spectrum reveals an obvious continuous absorption band in the wavelength range of 220-300 nm, which is mainly caused by the absorption of inorganic ions, such as phosphor, aluminum, sodium, potassium and barium, in phosphate glass.

3.2. Optical gain properties

A 275 nm laser and a 405 nm laser were respectively used to excite the phosphate glass and the photoluminescence (PL) properties are presented in Fig. 3. Under the excitation of the laser, characteristic PL peaks at a wavelength of approximately 1535 nm were observed, and correspond to the $^4I_{13/2}\rightarrow{}^4I_{15/2}$ transition of Er^{3+} ions. It is expected that the high-efficiency excitation of Er^{3+}-Yb^{3+} co-doped phosphate glass may be achieved if a low-power blue-violet LED is used as the pump source. In this work, four LEDs with different central wavelengths (Yonglin Optoelectronics Co., Ltd), namely was 275 nm (YL-UVC275-6363), 365 nm (YL-UVALP-2835-365), 375 nm (YL-UVC-SMD2835-375), and 405 nm (YL-UVAHP-6060-405), were used as the pump sources. However, obvious optical gains were obtained in the waveguide only under the respective excitations of the 275 nm LED (32 mW/cm^2) and 405 nm LED (914 mW/cm^2). One reason for this is that the pump power densities of 365 nm LED (14.5 mW/cm^2) and 375 nm LED (12 mW/cm^2) were too low to reach the turn-on power required to generate gain. The turn-on power is defined as the pump power at which gain occurs. Optical gain could be achieved under the excitation of the 275 nm LED with low-power (32 mW/cm^2) primarily because the

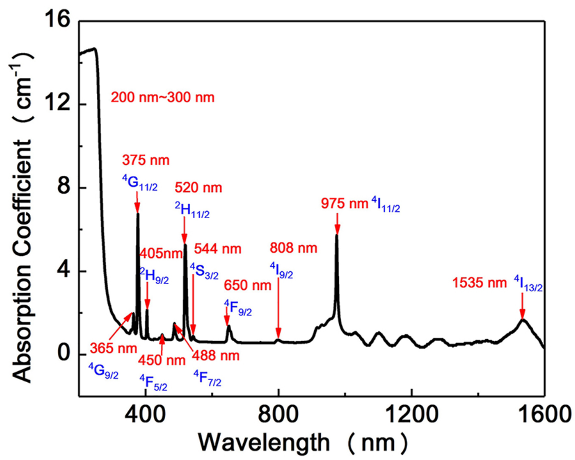

Fig. 2. The absorption spectrum of the phosphate glass. The absorption bands are attributed to the transitions from the ground state $^4I_{15/2}$ of Er^{3+} ions to the corresponding excited-state energy levels.

energy transfer effect between the inorganic ions in the phosphate glass and the Er^{3+} ions can help the Er^{3+} ions achieve the transition from the ground state to the excited state. Moreover, the relatively large absorption cross-section (3.141×10^{-24} m^{-2}) helps improve the absorption efficiency of the 275 nm LED. Although the absorption cross-section of 1.328×10^{-24} m^{-2} at the wavelength of 405 nm is smaller than that at 275 nm, optical gain could also be obtained due to the high pump power density of the 405 nm LED.

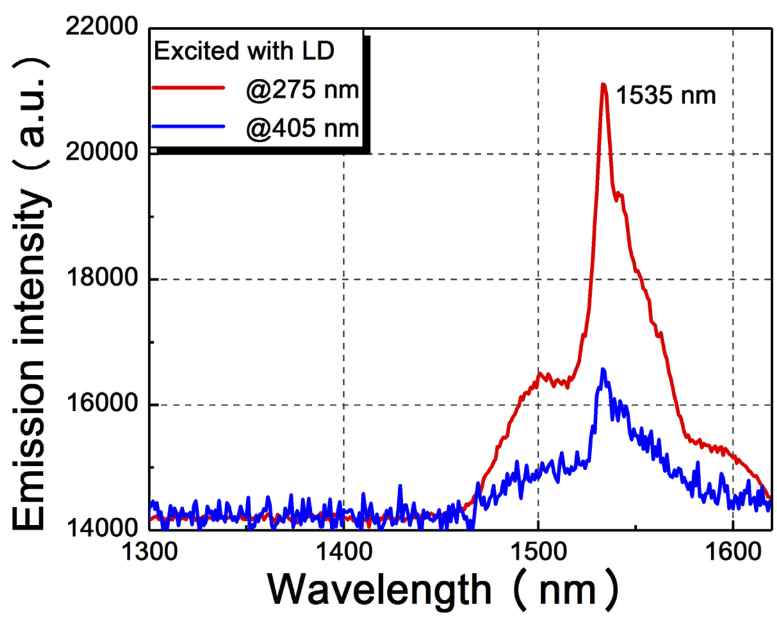

Fig. 3. The PL spectrum of the phosphate glass under the excitation of laser.

Via the use of the vertical top pumping mode of a blue-violet LED, the pump power can be uniformly distributed throughout the 10-mm-long planar waveguide, and can be continuously

Optics EXPRESS

supplemented during the transmission along the waveguide. The schematic diagram of gain measurement is illustrated in Fig. 4.

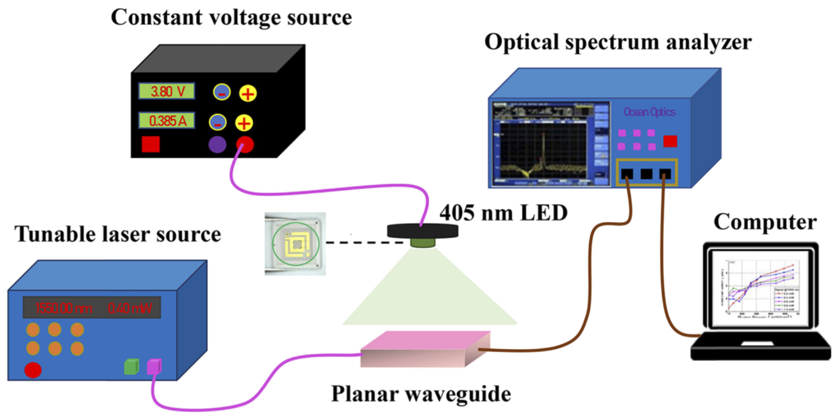

Fig. 4. The schematics of optical gain measurement. The wall-plug efficiency of the 405 nm LED is 40.3% at the rated power, and the viewing directionality is typically 110°.

The relationships between the internal optical gain at 1550 nm and different 405 nm LED pump power densities are shown in Fig. 5(a). At different input signal powers (0.2 to 1.0 mW), the variation trend and amplitude of the output signal power were relatively consistent, and increased with the increase of the pump power intensity. When the signal power was 0.2 mW and the pump power density was 914 mW/cm^2, the gain reached the maximum value of 5.2 dB. When the signal power was 0.4 mW, the turn-on pump power density was 190 mW/cm^2, and an internal optical gain of about 4.5 dB/cm was obtained. When the signal power was 0.4 mW and the pump power density was 914 mW/cm^2, the relative gain, internal gain, and net gain were respectively 7.6, 4.5, and 0.5 dB/cm (these gains are defined in section 4.2). As we know, the necessary condition for the generation of gain was that the number of Er^{3+} ions in the ground state $^4I_{15/2}$ and excited state $^4I_{13/2}$ was equal. When the pump power was higher than the turn-on power, there was enough inversion particles density, and the smaller the input signal was, the less inversion particles were consumed. Therefore, the gain was higher when the input signal was small when the pump power was greater than 300 mW/cm^2 in Fig. 5(a). However, when the pump power is below 300 mW/cm^2, the inversion particles density is small and the ability to generate gain is weak. So some other factors, such as loss of waveguide and thermal effect caused by pump source and so on cannot be ignored. The smaller the signal is, the more obvious the influence of these factors on the gain is. Therefore, it goes against the trend of pump power higher than 300 mW/cm^2.

As can be seen from Fig. 5(b), as the pump power density increased, the signal intensity at the wavelength of 1550 nm was significantly enhanced, and the wavelength range of excitation radiation was between 1450 and 1650 nm, thereby indicating that the planar waveguide could have a large bandwidth of amplification capability under 405 nm LED top-pumping.

Three emission peaks of Er^{3+} ions at 495, 545, and 694 nm were also observed in the wavelength range of 450-800 nm. Luminescence corresponding to the transitions of Er^{3+} ions from $^4F_{7/2}$ to $^4I_{15/2}$, $^2H_{9/2}$ to $^4I_{11/2}$, and $^2H_{9/2}$ to $^4I_{13/2}$, was respectively considered. The transition process of the Er^{3+} ions under 405 nm LED excitation can be described as follows. When Er^{3+} ions in the ground state $^4I_{15/2}$ absorbed the 405 nm pump energy and transitioned to the $^2H_{9/2}$ state, some ions rapidly underwent non-radiative transition to the $^4F_{7/2}$ state, from which they underwent radiative transition to the ground state level and generated 495 nm luminescence. Other ions in the $^2H_{9/2}$ state achieved luminescence at 694 and 545 nm via radiative transition from the

Optics EXPRESS

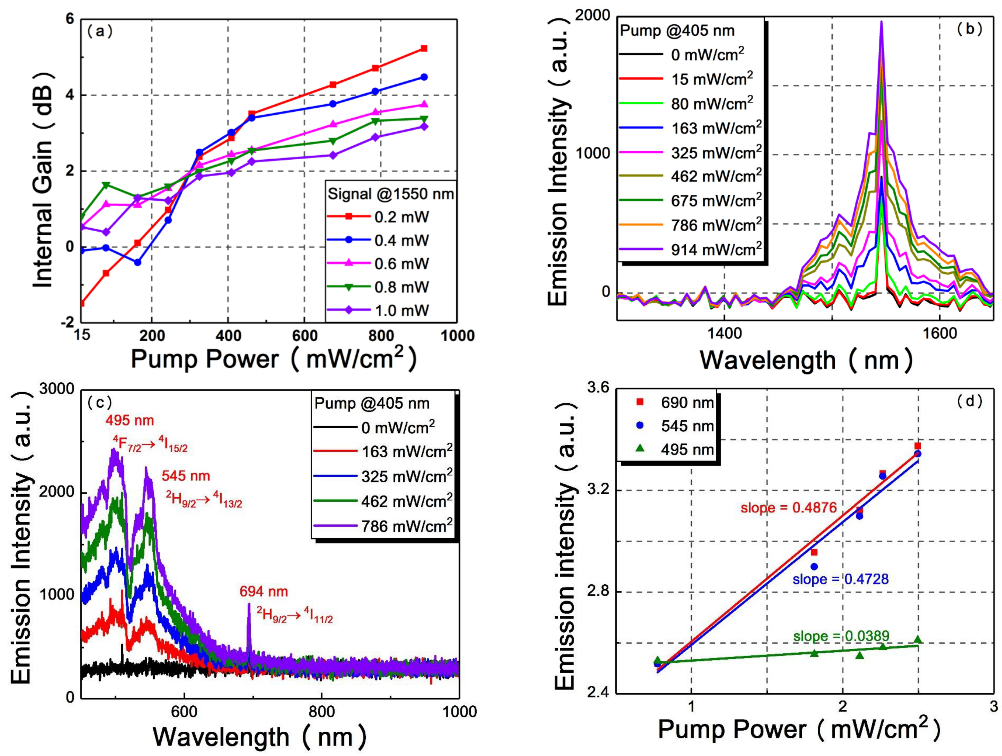

Fig. 5. (a)The internal gain under different 405 nm LED pump power densities. (b) The relationship between the signal intensity and different pump power densities when pumped by a 405 nm LED (the input signal power was 0.4 mW). (c) The down-conversion luminescence spectrum. (d) The logarithmic curve of the intensity of variation down-conversion luminescence with the pump power density.

$^2H_{9/2}$ state to the $^4I_{11/2}$ and $^4I_{13/2}$ states, respectively. On the other hand, the Er^{3+} ions that transitioned to the $^4I_{11/2}$ state underwent fast non-radiative transition to the $^4I_{13/2}$ state because of the shorter lifetime of the $^4I_{11/2}$ state (on the order of μs) and achieved luminescence at 1535 nm via radiative transition from the $^4I_{13/2}$ state to the ground state $^4I_{15/2}$. Although the emission of Er^{3+} ions at 545 nm also occurred under 405nm LED excitation, the luminescence was a type of Stokes light, and contributed to the emission at 1535 nm from the $^4I_{13/2}$ to the $^4I_{15/2}$ state. However, under 980 nm LD excitation, the emission of Er^{3+} ions at 545 nm was anti-Stokes light, which consumed the Er^{3+} ions at the $^4I_{11/2}$ level and decreased the emission of Er^{3+} ions at 1550 nm. Figure 5(c) presents the relationships between the luminescence intensity and different 405 nm pump power densities. It is evident that the luminescence intensities at 495, 545, and 694 nm increased with the increase of the pump power density. The relationship between the luminescence intensity I_{em} and pumping intensity I_{ex} can be defined as follows [22]:

$$I_{em} \propto (I_{ex})^n, \tag{1}$$

where n represents the proportion of the number of emitted photons that transitioned from the $^2H_{9/2}$ state to the lower energy level after absorbing a 405 nm photon. Figure 5(d) presents the logarithmic curve of the variation of the luminescence intensity of Er^{3+} ions at the emission peaks of 495, 545, and 694 nm with the pump power density. The slope fittings of the straight line were 0.4876, 0.4728, and 0.0389 respectively, indicating that 48.76%, 47.28%, and 3.89% of the Er^{3+} ions at the $^2H_{9/2}$ level respectively transitioned to the corresponding energy level.

The results demonstrate that nearly all the Er^{3+} ions transitioned from the $^2H_{9/2}$ state to the $^4I_{11/2}$, $^4I_{13/2}$, and $^4I_{15/2}$ states, among which the number of Er^{3+} ions that transitioned to the $^4I_{11/2}$ and $^4I_{13/2}$ states accounted for 51.17% of the total, and the Er^{3+} ions in these two levels both contributed to the luminescence at 1550 nm. Therefore, a good amplification effect can be achieved under 405 nm LED top-pumping.

A 275 nm LED was also used to excite the phosphate planar waveguide. Figure 6(a) presents the output signal at the wavelength of 1550 nm, from which it is evident that the intensity of the signal power was amplified by about 64.4% and 158.5% when the pump power density was 11 and 32 mW/cm^2, respectively. This equated to internal gains of about 2.2 and 4.1 dB/cm. Few publications have explained the causes of absorption before 300 nm in rare earth-doped materials. It is considered that there should be a process of energy transfer from the host material ions to the Er^{3+} ions in the phosphate glass under an excitation of 275 nm, which is similar to the energy transfer between Er^{3+} ions and Si nanocrystals, as well as that between organic ligands and rare earth-ions [23–25]. As presented in Fig. 6(b), a diagram of the energy transition in the phosphate glass was established to explain the energy transfer mechanism under 275 nm LED pumping. The inorganic ions in the phosphate glass at the ground state S_0 absorbed the pump energy of the 275 nm LED. They transitioned to the excited states S_1 at higher positions, and then jumped to excited states T_n at a lower position via intersystem crossing (ISC). The ions in the T_n state were unstable and rapidly transitioned to the lowest excited state T_1 via non-radiation transition. Some of the ions in the T_1 state radiated to S_0 and emitted phosphorescence, while others transferred energy to the $^4I_{13/2}$ level of Er^{3+} ions via resonance energy transfer (RET). Finally, the Er^{3+} ions in the $^4I_{13/2}$ level transitioned to the $^4I_{15/2}$ levels and achieved 1550 nm stimulated radiation. Optical gain can be obtained under low-power 275 nm LED pumping, which demonstrates that different types of LEDs can be used as pumping sources in the field of optical integration.

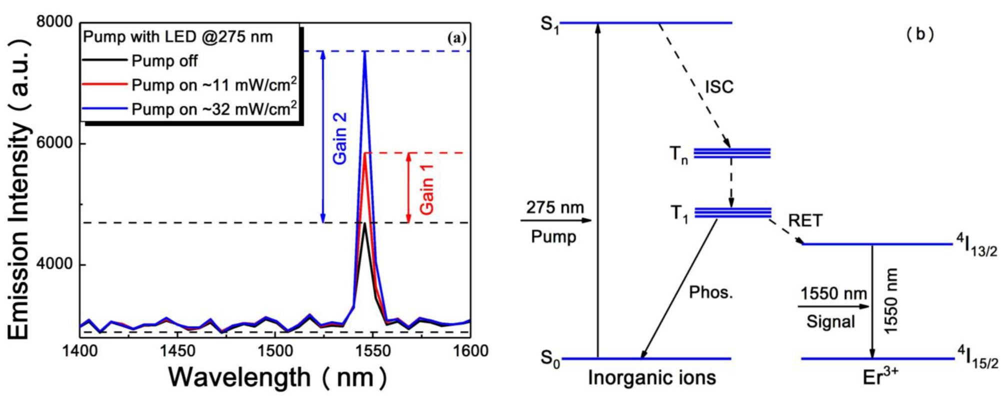

Fig. 6. (a)The output signal intensity with and without 275 nm LED pumping. The black line represents the input signal power of 0.4 mW. (b) The energy transfer process of inorganic ions and Er^{3+} ions under the excitation of a 275 nm LED.

4. Theoretical basis

4.1. Nonlinear rate and power propagation equations

Under excitation of 405 nm LED, there is almost no corresponding intrinsic absorption state of Yb^{3+} ions [26,27], and the intrinsic absorption of Er^{3+} ions from the $^4I_{15/2}$ to the $^2H_{9/2}$ state plays an important role. The simplified energy levels diagram of the Er^{3+}-Yb^{3+} co-doped system is established in Fig. 7.

Optics EXPRESS

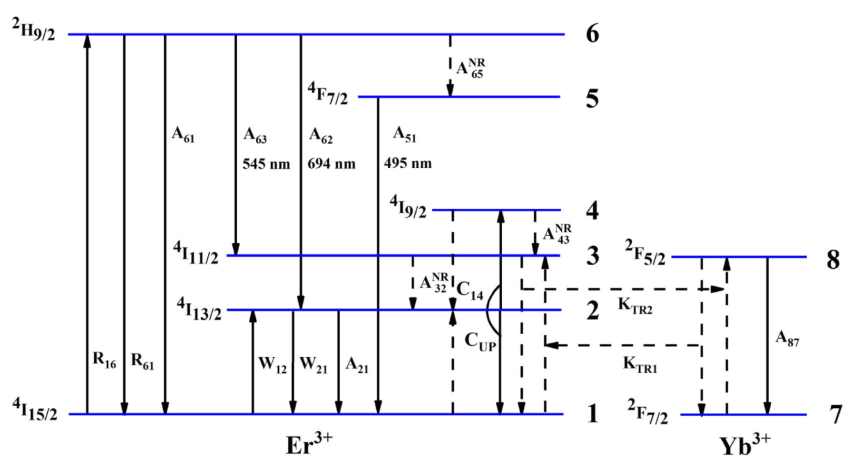

Fig. 7. The simplified energy levels diagram of Er^{3+}-Yb^{3+} co-doped system. The arrows represent the processes included in the rate equations used for the calculations. The dotted arrow represents the spontaneous non-radiative transition.

The average populations of the Er^{3+} levels $^4I_{15/2}$, $^4I_{13/2}$, $^4I_{11/2}$, $^4I_{9/2}$, $^4F_{7/2}$, $^2H_{9/2}$, and of the Yb^{3+} levels $^2F_{7/2}$ and $^2F_{5/2}$ are presented by N_1, N_2, N_3, N_4, N_5, N_6, N_7, and N_8, respectively. In particular, the following transitions are considered: 1) pump absorption and stimulated emission between the $^4I_{15/2}$ and $^2H_{9/2}$ states of Er^{3+} ions, 2) signal absorption and stimulated emission between the $^4I_{15/2}$ and $^4I_{13/2}$ states of Er^{3+} ions, 3) spontaneous decay from the $^2H_{9/2}$, $^4F_{7/2}$, $^4I_{9/2}$, $^4I_{11/2}$, and $^4I_{13/2}$ states of Er^{3+} ions: $^2H_{9/2}\rightarrow{}^4F_{7/2}$ (A_{65}^{NR}), $^4I_{11/2}$ (A_{63}), $^4I_{13/2}$ (A_{62}), $^4I_{15/2}$ (A_{61}), $^4F_{7/2}\rightarrow{}^4I_{15/2}$ (A_{51}), $^4I_{9/2}\rightarrow{}^4I_{11/2}$ (A_{43}^{NR}), $^4I_{11/2}\rightarrow{}^4I_{13/2}$ (A_{32}^{NR}), $^4I_{13/2}\rightarrow{}^4I_{15/2}$ (A_{21}), 4) uniform cooperative upconversion between a pair of excited erbium ions: $^4I_{13/2}$ +$^4I_{13/2}$ $\rightarrow{}^4I_{15/2}$ +$^4I_{9/2}$, 5) cross–relaxation process taking place between the two neighboring erbium ions: $^4I_{15/2}$ +$^4I_{9/2}$ $\rightarrow{}^4I_{13/2}$, 6) forward energy transfer process between Yb^{3+} ions and Er^{3+} ions: $^2F_{5/2}$ +$^4I_{15/2}\rightarrow{}^2F_{7/2}$ +$^4I_{11/2}$, and backward energy transfer process between Er^{3+} ions and Yb^{3+} ions: $^2F_{7/2}$ +$^4I_{11/2}\rightarrow{}^2F_{5/2}$ +$^4I_{15/2}$, 7) spontaneous decay from the $^2F_{5/2}$ state of Yb^{3+} ions:$^2F_{5/2}\rightarrow{}^2F_{7/2}$ (A_{87}). As a result, the steady-state rate equations for the Er^{3+}-Yb^{3+} co-doped system can be written as:

$$\frac{dN_1}{dt} = -(W_{12}+R_{16})N_1 + (W_{21}+A_{21})N_2 + A_{51}N_5 + (R_{61}+A_{61})N_6 + C_{UP}{N_2}^2 - C_{14}N_1N_4 - K_{TR1}N_1N_8 + K_{TR2}N_3N_7, \tag{2}$$

$$\frac{dN_2}{dt} = W_{12}N_1 - (W_{21}+A_{21})N_2 + A_{32}^{NR}N_3 + A_{62}N_6 - 2C_{UP}{N_2}^2 + 2C_{14}N_1N_4, \tag{3}$$

$$\frac{dN_3}{dt} = -A_{32}^{NR}N_3 + A_{43}^{NR}N_4 + A_{63}N_6 + K_{TR1}N_1N_8 - K_{TR2}N_3N_7, \tag{4}$$

$$\frac{dN_4}{dt} = -A_{43}^{NR}N_4 + C_{UP}{N_2}^2 - C_{14}N_1N_4, \tag{5}$$

$$\frac{dN_5}{dt} = -A_{51}N_5 + A_{65}^{NR}N_6, \tag{6}$$

$$N_{Er} = N_1 + N_2 + N_3 + N_4 + N_5 + N_6, \tag{7}$$

$$\frac{dN_8}{dt} = -A_{87}N_8 - K_{TR1}N_1N_8 + K_{TR2}N_3N_7, \tag{8}$$

Optics EXPRESS

$$N_{Yb} = N_7 + N_8, \tag{9}$$

where A_{ji}, A_{ji}^{NR} are the radiative decay rate and non-radiative decay rate from level j to i, respectively. C_{UP} is the cooperative upconversion coefficients. C_{14} is the cross-relaxation coefficient of Er^{3+} ions from $^4I_{15/2}$ and $^4I_{9/2}$ states to $^4I_{11/2}$ state in Er^{3+} ions. K_{TR1} and K_{TR2} are the forward and backward energy transfer coefficients from Yb^{3+} to Er^{3+} ions. N_{Er} and N_{Yb} represent the concentrations of Er^{3+} and Yb^{3+} ions. The stimulated emission and absorption transition rates of signal and pump wavelength, W_{ij} and R_{ij}, are given by:

$$W_{12/21} = \frac{\sigma_{a12/e21} P_S(Z) \lambda_S}{hca} \Gamma_S, \tag{10}$$

$$R_{16/61} = \frac{\sigma_{a16/e61} P_P(Z) \lambda_P}{hca} \Gamma_P, \tag{11}$$

where h is Planck constant. c is the speed of light. *a* is the area of the waveguide's cross-section. $P_S(Z)$ and $P_P(Z)$ are the optical powers of signal and pump light at waveguide position Z, respectively. σ_{a12}, σ_{e21} are the stimulated absorption cross-section and emission cross-section of Er^{3+} ions to signal light. λ_S and λ_P are the wavelengths of signal and pump, respectively. σ_{a16}, σ_{e61} represent the stimulated absorption cross-section and emission cross-section of Er^{3+} ions to pump light. Γ_P and Γ_S are the overlapping integral factors, which depend on the optical field distribution of the pump and signal lights. They can be expressed as [28]:

$$\Gamma_{P,S} = \iint_a \Psi_{P,S}(x,y) f(x,y) dxdy, \tag{12}$$

where *f(x,y)* is the normalized doping distribution function of Er^{3+} ions. Assuming the Er^{3+} ions doped in phosphate glass is uniform, *f(x,y)* is 1. The $\Psi_{P,S}(x,y)$ is the normalized function of pump and signal intensity distribution. Combined with the relative permittivity distribution, the transverse Helmholtz equations of waveguide regions can be written, and the field distribution of the waveguide can be obtained.

The Er^{3+} ions absorption cross-section is obtained from the absorption spectrum of Fig. 2 by using the following equation:

$$\sigma_{aij}(\lambda_k) = \frac{\alpha(\lambda)}{\Gamma_S N_{Er}}, \tag{13}$$

where $\alpha(\lambda)$ is absorption coefficient.

The stimulated Er^{3+} emission cross-section can be calculated using the McCumber theory [29,30]:

$$\sigma_{eij}(\lambda_k) = \sigma_{aij}(\lambda_k) exp\left(\frac{\varepsilon - \frac{hc}{\lambda}}{KT}\right), \tag{14}$$

where ε is the effective energy difference between the upper and lower field states obtained from the highest absorption peak of Er^{3+} ions, T is the absolute temperature, and K is the Boltzmann constants.

The optical power transmission equations of signal and pump power can be described as follows:

$$\frac{dP_S(Z)}{dZ} = -\Gamma_S[\sigma_{a12}(\lambda_S)N_1(Z) - \sigma_{e21}(\lambda_S)N_2(Z) + \alpha_S]P_S(Z), \tag{15}$$

$$\frac{dP_P(Z)}{dZ} = -\Gamma_P[\sigma_{a15}(\lambda_P)N_1(Z) - \sigma_{e51}(\lambda_P)N_5(Z) + \alpha_P]\ P_P(Z) + P_P\ , \tag{16}$$

The boundary conditions of signal and pump power are $P_S(0)$ and $P_P(0)$, respectively. Here $P_S(0)$ is 0.4 mW, and $P_P(0)$ is 0. Where α_S, α_P are the propagation losses of the signal and pump lights. L is the waveguide length. P_P is the pump power at the simulated unit step length Z.

The pump power is considered to be evenly distributed along the whole waveguide. A pump power of P_P is added at each step Z when using Runge-Kutta algorithm to calculate $P_P(Z)$. This is different from 980 nm pumping mode, which is coupled from one end of the waveguide and the power is gradually attenuated along the transmission direction of the waveguide.

4.2. Gain defined and choice of parameters

The transmission of optical power and calculation process of gain is shown in Fig. 8. The net gain $G(L)_{net}$, internal gain $G(L)_{int}$, and relative gain $G(L)_{rel}$ are defined as follows [31]:

$$G(L)_{net} = 10Lg\left[\frac{P_s(L)}{P_0(0)}\right],\quad G(L)_{int} = 10Lg\left[\frac{P_s(L)}{P_s(0)}\right],\quad G(L)_{rel} = 10Lg\left[\frac{P_s(L)}{P_{s0}(L)}\right], \tag{17}$$

where $P_S(0)$ is the signal power at the input of the waveguide. $P_S(L)$, $P_{S0}(L)$ are the signal powers at the output of the waveguide with and without pump power, respectively. $P_0(0)$ is the output power of signal laser.

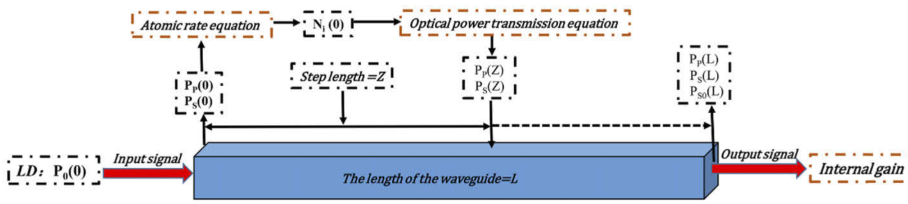

Fig. 8. The diagram of calculation process of theoretical simulation of gain.

The relationship between the above three gains is approximated as:

$$G(L)_{rel} = G(L)_{int} + \alpha_{abs} + \alpha_{tra},\; G(L)_{int} = G(L)_{net} + 2\alpha_{cou}, \tag{18}$$

where α_{abs} and α_{tra} are the absorption loss and transmission loss of waveguide. α_{cou} is the coupling loss between a channel waveguide and a fiber. By measuring $P_S(L)$, $P_{S0}(L)$, $P_S(0)$, and $P_0(0)$, the experimental values of gains can be obtained and the sum of α_{abs} and α_{tra} can be caculated as 3.1 dB/cm. The α_{cou} is 2.0 dB. Parameters used to simulate gain performance are listed in Table 1. The values of some parameters, such as α_S, α_P, C_{14}, K_{TR}, and $A_{87,}$ are given in Ref. [32].

4.3. Results and discussion

Figure 9(a) compares the internal gain under 405 nm intrinsic excitation at different waveguide lengths. For the waveguides with lengths of 1, 2, 3, and 4 cm, the internal gain was respectively 4.1, 8.5, 12.2, and 14.8 dB. The results demonstrate that the longer the waveguide, the higher the gain that could be achieved under the same pump power density. Compared with the gain of 4.5 dB produced by 914 mW/cm^2, 405 nm LED pumping in the experiment, the optical gain of 4.1 dB was obtained in the simulation, and is therefore in accordance with the experimental results. In addition, for the waveguides with lengths of 1, 2, and 3 cm, the turn-on pump power density was 56, 41, and 36 mW/cm^2, respectively. This result can be explained from the perspective of population inversion.

Figure 9(b) presents the population of Er^{3+} ions at the ground state $^4I_{15/2}$ and the metastable state $^4I_{13/2}$ as a function of pump power. One of the necessary conditions for the generation of optical gain is population inversion, which requires that the ion concentrations in the metastable state N_2 be comparable with the ion concentrations in the ground state N_1. When the pump power density is low, the pumping energy is not sufficient to excite Er^{3+} ions from the ground

Research Article | Vol. 29, No. 8 / 12 April 2021 / Optics Express 11382
Optics EXPRESS

Table 1. Parameters used for modeling Er^{3+}-Yb^{3+} co-doped phosphate planar waveguide.

Parameter	Symbol	Value
Er^{3+} ions concentration	N_{Er}	1.616×10^{26} ions/m^3
Yb^{3+} ions concentration	N_{Yb}	3.14×10^{26} ions/m^3
pump wavelength	λ_P	405 nm
signal wavelength	λ_S	1550 nm
signal power	$P_S(0)$	0.4 mW
cross-section of waveguide core	a	9 μm×9 μm
transmission loss at 1550 nm	α_S	0.5 dB/cm [32]
transmission loss at 405 nm	α_P	0.5 dB/cm [32]
waveguide length	L	1 cm
cooperative upconversion coefficient	C_{UP}	6×10^{-25} m^3/s
Er^{3+} ions cross-relaxation coefficient	C_{14}	8×10^{-25} m^3/s [32]
Yb^{3+} ions to Er^{3+} ions energy transfer coefficients	K_{TR1}	7×10^{-23} m^3/s [32]
Er^{3+} ions to Yb^{3+} ions energy transfer coefficients,	K_{TR2}	1×10^{-23} m^3/s [32]
over-lapping integral factor at 1550 nm	Γ_S	0.627
0ver-lapping integral factor at 405 nm	Γ_P	0.637
stimulated absorption cross-section (1550 nm)	σ_{a12}	1.029×10^{-24} m^2
stimulated emission cross-section (1550 nm)	σ_{e21}	1.691×10^{-24} m^2
stimulated absorption cross-section (405 nm)	σ_{a16}	1.328×10^{-24} m^2
stimulated emission cross-section (405 nm)	σ_{e61}	1.328×10^{-24} m^2
Er^{3+} ions spontaneous radiation incidence: $^4I_{13/2} \rightarrow {}^4I_{15/2}$	A_{21}	100.33 s^{-1}
$^4I_{11/2} \rightarrow {}^4I_{13/2}$	A_{32}^{NR}	21.91 s^{-1}
$^4I_{9/2} \rightarrow {}^4I_{11/2}$	A_{43}^{NR}	2.77 s^{-1}
$^4F_{7/2} \rightarrow {}^4I_{15/2}$	A_{51}	1943.85 s^{-1}
$^2H_{9/2} \rightarrow {}^4I_{15/2}$	A_{61}	732.98 s^{-1}
$^2H_{9/2} \rightarrow {}^4I_{13/2}$	A_{62}	1054.30 s^{-1}
$^2H_{9/2} \rightarrow {}^4I_{11/2}$	A_{63}	289.22 s^{-1}
$^2H_{9/2} \rightarrow {}^4F_{7/2}$	A_{65}^{NR}	8.34 s^{-1}
Yb^{3+} ions spontaneous radiation incidence: $^2F_{5/2} \rightarrow {}^2F_{7/2}$	A_{87}	714.29 s^{-1} [32]

state $^4I_{15/2}$ to the metastable state $^4I_{13/2}$, so the necessary condition of population inversion cannot achieved. For the 10-mm-long waveguide, the values of N_1 and N_2 were equal when the pump power density reached 56 mW/cm^2, and optical gain started to be generated. With the increase of the waveguide length, the number of times that P_P increased, and the total pump power accumulated in the waveguide were higher. Thus, it was easier to realize the inversion of the number of particles, and the corresponding turn-on power decreased. This is different from the traditional model under 980 nm LD pumping, the optical field of which gradually attenuates along the waveguide direction and the turn-on pump power of which increases with the increase of the waveguide length [33].

The relationship between the stimulated absorption cross-section at 405 nm and optical gain is exhibited in Fig. 9(c). The turn-on pump power density decreased from 290 to 51 mW/cm^2 as the stimulated absorption cross-section at 405 nm increased from 0.328×10^{-24} to 1.828×10^{-24} m^2. When the stimulated absorption cross-section increased by 4.5 times, the turn-on pump power density was correspondingly reduced by nearly 4.7 times. This is because the larger

Optics EXPRESS

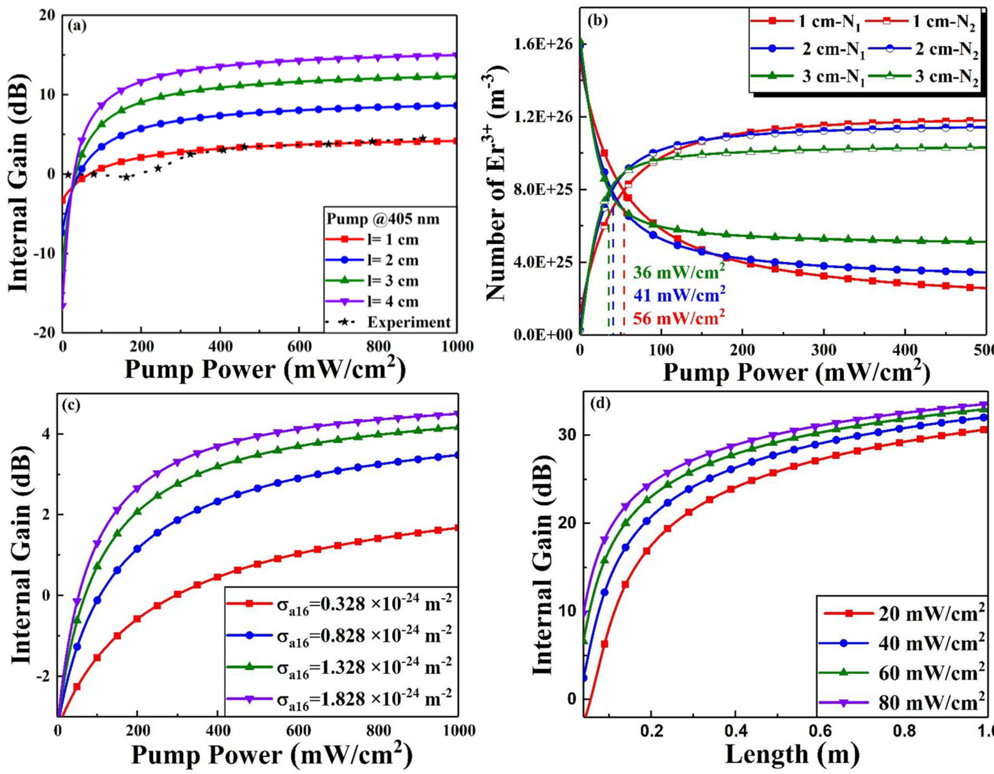

Fig. 9. (a) The internal gain as a function of the pump power density for different waveguide lengths. (b) The population of Er^{3+} ions in the ground state and the metastable state as a function of the pump power density under 405 nm excitation. (c) The internal gain as a function of pump power density for different stimulated absorption cross-sections. (d) The internal gain as a function of the waveguide length for different pump power densities.

the stimulated absorption cross-section of Er^{3+}ions, the higher the absorption efficiency of the material for the pump light. This result can provide concept for the research of complex organic erbium doped polymer optical waveguide amplifiers. In general, the absorption cross-section of organic ligands at 405 nm is between 10^{-22} and 10^{-23} m^2, which is about 2 orders of magnitude larger than the intrinsic absorption cross-section of inorganic Er^{3+} ions [34]. This means that if a 405 nm LED is used to pump organic EDWAs, the turn-on pump power can be reduced by about 2 orders of magnitude as compared with 980 nm laser pumping [24,35]. Furthermore, sufficient energy can be absorbed via energy transfer between organic ligands and Er^{3+} ions to facilitate organic EDWAs to achieve higher optical gain.

Figure 9(d) presents the internal gain as a function of the waveguide length at different pump power densities, from which it can be seen that the gain can be continuously increased on a 10-cm-long device. Gaines of about 8.0 and 19.2 dB were respectively obtained under low-pump power densities of 20 and 80 mW/cm^2, respectively. When the length of the waveguide reaches 1 m, the internal gain reaches saturation, and gradually increases from 30.7 dB to 33.6 dB under different pump power densities. The power of the LED was uniformly distributed in the waveguide and it did not decrease along the waveguide direction; thus, the signal could be gradually amplified. In summation, the simulation results demonstrate that the disadvantages caused by a 980 nm LD can be overcome if the EYDWA is pumped by LEDs. Therefore, the new pumping mode afforded by LEDs will play an important role in optical communication and integration.

5. Conclusion

In this research, the absorption and PL properties of Er^{3+}-Yb^{3+} co-doped phosphate glass were investigated. The PL peak at a wavelength of 1550 nm corresponding to the $^4I_{13/2}\rightarrow{}^4I_{15/2}$ transition of Er^{3+} ions was observed. Via experimental comparison and theoretical simulation, a novel strategy was demonstrated for the achievement of the high optical gain of the planar waveguide via low-power commercial LED pumping. In an experiment, an internal optical gain of 5.2 dB/cm in a phosphate planar waveguide was obtained when pumped by a 914 mW/cm^2, 405 nm LED. It proved that 51.17% of the total Er^{3+} ions in the $^2H_{9/2}$ state contributed to the luminescence at a wavelength of 1550 nm. The intrinsic absorption of Er^{3+} ions at a wavelength of 405 nm was found to have a good effect on the amplification of the 1550 nm signal. An optical gain of 4.1 dB/cm was also obtained under 275 nm LED pumping at 32 mW/cm^2. Furthermore, a theoretical model for the gain calculation of 405 nm LED top-pumping was established. The relationships between different parameters and the optical gain were also discussed. The calculation results demonstrated that LED top-pumping can effectively compensate for the decreased pump intensity due to the transmission loss of the waveguide, and a calculated internal optical gain of 4.1 dB was obtained on a 10-mm-long device, which was in agreement with the experimental results. The optical gain achieved by commercial and convenient LED top-pumping will undoubtedly open a new direction for the development of optical integration.

Funding. National Natural Science Foundation of China (61875170, 61107023); Principal's Fund of Xiamen University (20720150086).

Disclosures. The authors declare no conflicts of interest.

Supplemental document. See Supplement 1 for supporting content.

References

1. A. Q. Le Quang, R. Hierle, J. Zyss, I. Ledoux, G. Cusmai, R. Costa, A. Barberis, and S. M. Pietralunga, "Demonstration of net gain at 1550 nm in an erbium-doped polymersingle mode rib waveguide," Appl. Phys. Lett. **89**(14), 141124 (2006).
2. H. S. Han, S. Y. Seo, and J. H. Shin, "Optical gain at 1.54 µm in erbium-doped silicon nanocluster sensitized waveguide," Appl. Phys. Lett. **79**(27), 4568–4570 (2001).
3. S. A. Vazquez-Cordova, S. Aravazhi, C. Grivas, Y. S. Yong, S. M. Garcia-Blanco, J. L. Herek, and M. Pollnau, "High optical gain in erbium-doped potassium double tungstate channel waveguide amplifiers," Opt. Express **26**(5), 6260–6266 (2018).
4. J. Ronn, J. Zhang, W. Zhang, Z. Tu, A. Matikainen, X. Leroux, E. Duran-Valdeiglesias, N. Vulliet, F. Boeuf, C. Alonso-Ramos, H. Lipsanen, L. Vivien, Z. Sun, and E. Cassan, "Erbium-doped hybrid waveguide amplifiers with net optical gain on a fully industrial 300 mm silicon nitride photonic platform," Opt. Express **28**(19), 27919–27926 (2020).
5. D. Zhang, C. Chen, C. Chen, C. Ma, D. Zhang, S. Bo, and Z. Zhen, "Optical gain at 1535 nm in LaF_3:Er,Yb nanoparticle-doped organic-inorganic hybrid material waveguide," Appl. Phys. Lett. **91**(16), 161109 (2007).
6. J. D. Marconi, M. L. F. Abbade, C. M. Serpa-Imbett, and E. A. M. Fagotto, "Ultra-broadband two-pump optical parametric amplifier in tellurite waveguides with engineered dispersion," Opt. Express **25**(4), 4268–4283 (2017).
7. S. A. Vazquez-Cordova, M. Dijkstra, E. H. Bernhardi, F. Ay, K. Worhoff, J. L. Herek, S. M. Garcia-Blanco, and M. Pollnau, "Erbium-doped spiral amplifiers with 20 dB of net gain on silicon," Opt. Express **22**(21), 25993–26004 (2014).
8. Y. Zhang, P. Lv, D. Wang, Z. Qin, F. Wang, D. Zhang, D. Zhao, G. Qin, and W. Qin, "$KMnF_3$:Yb^{3+},Er^{3+} Core-Active-Shell Nanoparticles with Broadband Down-Shifting Luminescence at 1.5 µm for Polymer-Based Waveguide Amplifiers," Nanomaterials 9 (2019).
9. D. Przybylska and T. Grzyb, "Synthesis and up-conversion of core/shell SrF_2:Yb^{3+},Er^{3+}@SrF_2:Yb^{3+},Nd^{3+} nanoparticles under 808, 975, and 1532 nm excitation wavelengths," J. Alloys Compd. **831**, 154797 (2020).
10. L. Mescia, S. Girard, P. Bia, T. Robin, A. Laurent, F. Prudenzano, A. Boukenter, and Y. Ouerdane, "Optimization of the Design of High Power Er^{3+}/Yb^{3+}-Codoped Fiber Amplifiers for Space Missions by Means of Particle Swarm Approach," IEEE J. Sel. Top. Quantum Electron. **20**(5), 484–491 (2014).

Optics EXPRESS

11. M. Zhang, W. Zhang, F. Wang, D. Zhao, C. Qu, X. Wang, Y. Yi, E. Cassan, and D. Zhang, "High-gain polymer optical waveguide amplifiers based on core-shell $NaYF_4$/$NaLuF_4$: Yb^{3+}, Er^{3+} NPs-PMMA covalent-linking nanocomposites," Sci. Rep. **6**(1), 36729 (2016).
12. Y. Yang, F. Wang, S. Ma, M. Zhou, Y. Lang, G. Qin, D. Zhang, W. Qin, D. Zhao, and X. Zhang, "Great enhancement of relative gain in polymer waveguide amplifier using $NaYF_4$/$NaLuF_4$:Yb,Er-PMMA nanocomposite as gain media," Polymer **188**, 122104 (2020).
13. C. Chen, D. Zhang, T. Li, D. M. Zhang, L. M. Song, and Z. Zhen, "Erbium-ytterbium codoped waveguide amplifier fabricated with solution-processable complex," Appl. Phys. Lett. **94**(4), 041119 (2009).
14. A. Ladaci, S. Girard, L. Mescia, T. Robin, A. Laurent, B. Cadier, M. Boutillier, Y. Ouerdane, and A. Boukenter, "Optimized radiation-hardened erbium doped fiber amplifiers for long space missions," J. Appl. Phys. **121**(16), 163104 (2017).
15. M. Yuan, R. Wang, C. Zhang, Z. Yang, W. Cui, X. Yang, N. Xiao, H. Wang, and X. Xu, "Exploiting the silent upconversion emissions from a single β-$NaYF_4$:Yb/Er microcrystal via saturated excitation," J. Mater. Chem. C **6**(38), 10226–10232 (2018).
16. T. Sakimura, K. Hirosawa, Y. Watanabe, T. Ando, S. Kameyama, K. Asaka, H. Tanaka, M. Furuta, M. Hagio, Y. Hirano, H. Inokuchi, and T. Yanagisawa, "1.55-µm high-peak, high-average-power laser amplifier using an Er,Yb:glass planar waveguide for wind sensing coherent Doppler lidar," Opt. Express **27**(17), 24175–24187 (2019).
17. J. Lee, J. H. Shin, and N. Park, "Optical gain at 1.5µm in nanocrystal Si sensitized, Er-doped silica waveguide using top-pumping 470 nm LED," J. Lightwave Technol. **23**(1), 19–25 (2005).
18. H. Lee, J. H. Shin, and N. Park, "Performance analysis of nanocluster-Si sensitized Er-doped waveguide amplifier using top-pumped 470 nm LED," Opt. Express **13**(24), 9881–9889 (2005).
19. R. Dahal, C. Ugolini, J. Y. Lin, H. X. Jiang, and J. M. Zavada, "Erbium-doped GaN optical amplifiers operating at 1.54 µm," Appl. Phys. Lett. **95**(11), 111109 (2009).
20. L. Li, J. Zheng, Y. Zuo, B. Cheng, and Q. Wang, "Efficient 1.54-µm emission through Eu^{2+} sensitization of Er^{3+} in thin films of Eu^{2+}/ Er^{3+} codoped barium strontium silicate under broad ultraviolet light excitation," J. Lumin. **157**, 193–196 (2015).
21. W. T. Carnall, P. R. Fields, and K. Rajnak, "Electronic Energy Levels in the Trivalent Lanthanide Aquo Ions. I. Pr^{3+}, Nd^{3+}, Pm^{3+}, Sm^{3+}, Dy^{3+}, Ho^{3+}, Er^{3+}, and Tm^{3+}," J. Chem. Phys. **49**(10), 4424–4442 (1968).
22. X. Qiao, X. Fan, and M. Wang, "Spectroscopic properties of Er^{3+} doped glass ceramics containing Sr_2GdF_7 nanocrystals," Appl. Phys. Lett. (2006).
23. J. Bradley and M. Pollnau, "Erbium-doped integrated waveguide amplifiers and lasers," Laser Photonics Rev. **5**(3), 368–403 (2011).
24. H. Q. Ye, Z. Li, Y. Peng, C. C. Wang, T. Y. Li, Y. X. Zheng, A. Sapelkin, G. Adamopoulos, I. Hernandez, P. B. Wyatt, and W. P. Gillin, "Organo-erbium systems for optical amplification at telecommunications wavelengths," Nat. Mater. **13**(4), 382–386 (2014).
25. O. H. Park, S. Y. Seo, and B. S. Bae, "Indirect excitation of Er^{3+} in sol-gel hybrid films doped with an erbium complex," Appl. Phys. Lett. **82**(17), 2787–2789 (2003).
26. X. Zou and H. Toratani, "Evaluation of spectroscopic properties of Yb^{3+} -doped glasses," Phys. Rev. B Condens. Matter **52**, 15889–15897 (1995).
27. K. Lu and N. K. Dutta, "Spectroscopic properties of Yb-doped silica glass," J. Appl. Phys. **91**(2), 576–581 (2002).
28. D. Zhang, X. Li, X. Huang, S. Liu, H. Fu, K. Che, and L. Wang, "Optical Amplification at 1064 nm in $Nd(TTA)_3(TPPO)_2$ Complex Doped SU-8 Polymer Waveguide," IEEE Photonics J. **7**(5), 1–7 (2015).
29. D. E. McCumber, "Einstein Relations Connecting Broadband Emission and Absorption Spectra," Phys. Rev. **136**(4A), A954–A957 (1964).
30. R. M. Martin and R. S. Quimby, "Experimental evidence of the validity of the McCumber theory relating emission and absorption for rare-earth glasses," J. Opt. Soc. Am. B **23**(9), 1770–1775 (2006).
31. D.-L. Zhang, P.-R. Hua, and E. Y. B. Pun, "Correct determination of net gain in Er-doped optical waveguide amplifier from pump-on/off measurement," Opt. Commun. **279**(1), 64–67 (2007).
32. K. Liu and E. Y. B. Pun, "Modeling and experiments of packaged Er^{3+}–Yb^{3+} co-doped glass waveguide amplifiers," Opt. Commun. **273**(2), 413–420 (2007).
33. A. Shooshtari, T. Touam, S. I. Najafi, S. Safavi-Naeini, and H. Hatami-Hanza, "Yb^{3+}sensitized Er^{3+}-doped waveguide amplifiers: a theoretical approach," Proc. SPIE **3278**, 149 (1998).
34. L. Slooff, A. van Blaaderen, A. Polman, G. Hebbink, S. Klink, F. Veggel, D. Reinhoudt, and J. W. Hofstraat, "Rare-earth doped polymers for planar optical amplifiers," J. Appl. Phys. **91**(7), 3955–3980 (2002).
35. H. Zhan, J. Zhang, W. Fan, B. P. Zhang, L. Y. Ying, G. H. Xie, Z. S. Lin, H. S. Chen, H. Long, Z. M. Zheng, Z. W. Zheng, H. Xu, and D. Zhang, "Optical properties of organic neodymium complex doped optical waveguides based on the intramolecular energy transfer effect," Opt. Mater. Express **10**(10), 2624–2635 (2020).